

## Dynamic Force Balances and Cell Shape Changes during Cytokinesis

Anirban Sain,<sup>1,\*</sup> Mandar M. Inamdar,<sup>2</sup> and Frank Jülicher<sup>3</sup>

<sup>1</sup>Physics Department, Indian Institute of Technology-Bombay, Powai, Mumbai 400076, India

<sup>2</sup>Department of Civil Engineering, Indian Institute of Technology-Bombay, Powai, Mumbai 400076, India

<sup>3</sup>Max-Planck-Institute for the Physics of Complex Systems Nöthnitzer Strasse 38, 01187 Dresden, Germany

(Received 11 September 2013; published 27 January 2015)

During the division of animal cells, an actomyosin ring is formed in the cell cortex. The contraction of this ring induces shape changes of the cell and the formation of a cytokinesis furrow. In many cases, a cell-cell interface forms that separates the two new cells. Here we present a simple physical description of the cell shape changes and the dynamics of the interface closure, based on force balances involving active stresses and viscous friction. We discuss conditions in which the interface closure is either axially symmetric or asymmetric. We show that our model can account for the observed dynamics of ring contraction and interface closure in the *C. elegans* embryo.

DOI: 10.1103/PhysRevLett.114.048102

PACS numbers: 87.16.A-, 87.17.Ee, 87.17.Rt

One of the fundamental aspects of life is the ability of cells to duplicate by cell division. During cytokinesis, the last stage of cell division, a cell is physically divided in two subvolumes. This happens by the constriction of a contractile ring below the cell membrane. This contractile ring is enriched in actin filaments and myosin molecular motors which interact to generate contractile stresses. Contraction of the ring generates a furrow at the equatorial plane of the cell, see Figs. 1(a) and 1(b). Ring constriction can lead to a vanishing radius of this furrow [Fig. 1(e)]. Alternatively, the ring can constrict further while separating from the furrow, leaving a planar interface where two membranes adhere between furrow and contractile ring [Fig. 1(c)]. In the following we use the term “septum” to refer to this planar interface separating the future daughters [1]. In the symmetric case, the septum is an annular ring of width  $\delta = r_0 - r$ . The septum increases in area as the ring radius  $r$  decreases during ring contraction while the initial furrow remains at a radius  $r_0$  [Figs. 1(f) and 1(g)].

Here we focus on the *C. elegans* embryo as a model system for cytokinesis for which the dynamics of the septum can be studied quantitatively [2–5]. We develop a physical description of the dynamics of the cytokinesis furrow driven by the active contraction of the actomyosin ring and governed by dynamic force balances. We show that the septum forms via a first order transition of the membrane shape. We describe the dividing cell as an object with liquidlike material properties subject to a volume constraint and to actively generated tension. The cell shape is represented by two spherical elements of radius  $R$  that meet along a circular line. This circle defines the plane in which the cytokinesis furrow contracts and the septum expands, see Fig. 1. For a rotationally symmetric furrow and septum, with respect to the cell division axis, the shape of the septum can be characterized by the radius  $r$ , which decreases as a function of time during cytokinesis, and the

width  $\delta$  of the septum, see Figs. 1(f) and 1(g). Note that in many cell division events, the septum forms asymmetrically, starting from one side of the initial furrow as discussed below, see Figs. 4(a) and 4(b) [3,4]. The angle between furrow plane and the plasma membrane is denoted  $\psi/2$ , see Fig. 1(f).

Static force balances can be discussed introducing a potential function for the outer membrane and the septum given by  $F = E + 2\pi r\Sigma$  where  $E = \sigma A + 2\sigma' A'$ . The areas of the outer cell membrane and of the septum [shaded in Fig. 1(f)], are denoted  $A$  and  $A'$ , respectively. The contraction of the inner radius of the septum is driven by the contractile ring with line tension  $\Sigma$ . The surface tension of the cell surface is  $\sigma$  and that of the septum, consisting of two membranes, is  $2\sigma'$ . Here we neglect for simplicity effects of confinement and we do not consider cortical flows that in general arise from gradients in contractile tension [6–8]. Such cortical flows towards the furrow could modify our boundary conditions for the flow velocity at the septum boundary at  $r = r_0$ .

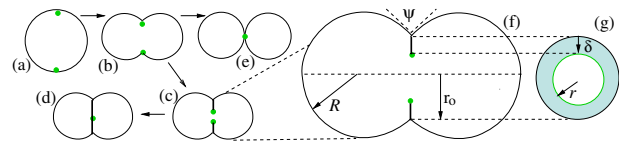


FIG. 1 (color online). Schematic representation of a dividing cell with axisymmetric geometry of the contractile process. The initial spherical cell (a) is deformed by the constriction of a contractile ring (b), shown as green dots in all the vertical sections. A septum forms (c). It shrinks to divide the cell (d). Division leading to vanishing contact area between the daughters (e). The geometry of the cell is characterized by two intersecting spheres of radius  $R$  which meet at an angle  $\psi$  (f). The septum has the shape of an annulus with inner and outer radii  $r$  and  $r + \delta$ , respectively (g).

We consider cell shape changes that occur at constant volume  $V = (4\pi/3)R_0^3$  [9], where  $R_0$  is the radius of the initial spherical cell. In this case, the configuration of the cell shape and the septum can be parametrized by the angle  $\psi \leq \pi$  and the inner radius  $r$  of the septum, see Fig. 1. The radius  $R$  and the width  $\delta$  of the septum follow from the geometric constraints  $r + \delta = R \sin(\psi/2)$  and  $R = R_0 \{1 + [1 + \sin^2(\psi/2)/2] \cos(\psi/2)\}^{-1/3}$ . If no septum forms,  $\delta = 0$  and  $r = r_{\max}$  with  $r_{\max} = R \sin(\psi/2)$ .

We define the dimensionless length ratios  $\bar{R} = R/R_0$ ,  $\bar{r} = r/R_0$ ,  $\bar{\delta} = \delta/R_0$  and we normalize the potential as  $\bar{F} = F/4\pi R_0^2 \sigma$  and define  $\bar{E}$  correspondingly. In the following we drop the bars on  $R$  and  $r$  to keep the notation simple. The potential reads

$$\bar{F}(\psi, r) = R^2 \left[ 1 + \cos\left(\frac{\psi}{2}\right) \right] + \frac{\bar{\sigma}}{2} \left[ R^2 \sin^2\left(\frac{\psi}{2}\right) - r^2 \right] + r\bar{\Sigma}, \quad (1)$$

where  $\bar{\sigma} = \sigma'/\sigma$  and  $\bar{\Sigma} = \Sigma/(2\sigma R_0)$ . The first and second term describe the contributions of surface tension of the outer membrane and the septum, respectively, while the last term describes the line tension of the contractile ring.

Static force balances correspond to values of  $r$  and  $\psi$  for which  $\partial \bar{E}/\partial \psi = 0$  and  $\partial \bar{E}/\partial r = -\bar{\Sigma}$ . For a given value of  $\bar{\sigma}$ , and for  $\bar{\delta} > 0$ , the first condition is satisfied for a particular value  $\psi = \psi_{\min}$ , where  $\cos(\psi_{\min}/2) = \bar{\sigma}$ . Note that  $\psi_{\min}$  is independent of  $r$ , as long as  $r < r_{\max} = R \sin(\psi_{\min}/2)$ .

The radius  $r$  is set by the line tension  $\bar{\Sigma}$  of the contractile ring. From  $-\bar{\Sigma} = \partial \bar{E}/\partial r$  it follows that the inner radius satisfies  $\bar{\Sigma} = \bar{\sigma}r$  for  $\delta > 0$  and  $\psi = \psi_{\min}$ . The sequence of shapes that is generated by ring contraction can be discussed by considering the potential  $\bar{F}(\bar{\Sigma}, \psi)$  as a function of the normalized line tension  $\bar{\Sigma}$ , for force balanced configurations, see Fig. 2. The figure reveals several branches of solutions. The black solid line describes the shapes without septum ( $\bar{\delta} = 0$ ). The lower branch of this line correspond to locally stable states, the higher branches to unstable states. For a certain value of the line tension  $\bar{\Sigma}_c(\bar{\sigma})$  which depends on the surface tension  $\bar{\sigma}$  of the septum, the shapes with  $\bar{\delta} = 0$  become unstable with respect to the formation of a septum. Unstable branches of states with new septum are shown as red, green, and blue lines, respectively, for different values of  $\bar{\sigma}$ . Formation of a septum occurs if  $\bar{\sigma} < 1$ . The closed state is again a locally stable state indicated by dashed lines. For given  $\bar{\sigma}$ , the branches of solutions form a Gibbs loop, corresponding to a first order shape transition [10]. The dynamics of expansion of the septum driven by the contraction of the inner ring requires a dynamic model involving dynamic force balances.

We now discuss the dynamics of the ring closure, expanding the septum. We assume that the area of the

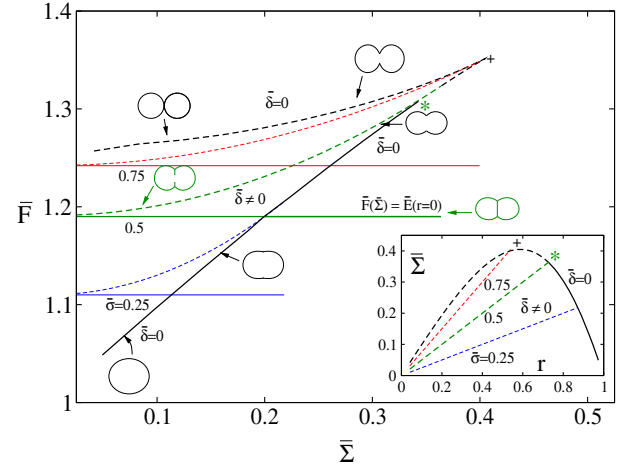


FIG. 2 (color online). Normalized energy  $\bar{F}$  as a function of normalized line tension  $\bar{\Sigma}$ , shown for three different values of normalized membrane tension  $\bar{\sigma}$  as indicated (colored lines). For  $\bar{\Sigma} = 0$ , the lowest energy shape is a sphere. Constricted shapes without formation of a septum correspond to the line with  $\bar{\delta} = 0$  (black). These shapes exhibit a furrow with increasingly strong indentation as  $\bar{\Sigma}$  increases. At the spinodal indicated “+”, the line folds back along a branch corresponding to locally unstable shapes (broken black line) until the radius  $\bar{r}$  vanishes at  $\bar{\Sigma} = 0$ . Lines corresponding to shapes with septum with  $\bar{\delta} \neq 0$  branch off (colored lines). The star denotes the point where the line  $\bar{\sigma} = 0.5$  (green) branches off the black line via the formation of a septum. The horizontal green line corresponds to the fully constricted state with  $r = 0$  for which the energy does not depend on  $\bar{\Sigma}$ . Similar curves are also shown for  $\bar{\delta} = 0.25$  (blue) and  $0.75$  (red). The intersection of the colored solid lines corresponding to fully constricted states with the black solid  $\bar{\delta} = 0$  line marks a first order transition point where the fully constricted state becomes energetically favored. The inset shows the normalized line tension  $\bar{\Sigma}$  as a function of normalized ring radius  $r$  for the values of  $\bar{\sigma}$  indicated.

septum can increase by local addition of material, for example via the fusion of vesicles that arrive from the cytoplasm [11]. We write dynamic equations that take into account viscous stresses and dynamic force balance. For a symmetric septum, the system has rotational symmetry and the flow profile  $v_\rho(\rho)$  in the septum is a function of the distance  $\rho$  from the center only. The nonvanishing components of the 2D viscous stress tensor are  $\sigma_{\rho\rho} = \sigma_0 + 2\eta(\partial v_\rho/\partial \rho)$ ,  $\sigma_{\theta\theta} = \sigma_0 + 2\eta(v_\rho/\rho)$ , where  $\sigma_0$  is the isotropic stress in the septum. A surface tension of the septum corresponds to positive  $\sigma_0 = 2\sigma'$ . Inserting these expressions for the stress in the force balance equation  $\partial_\rho \sigma_{\rho\rho} + \rho^{-1}(\sigma_{\rho\rho} - \sigma_{\theta\theta}) = 0$  we get an equation for the velocity profile,  $2\eta \partial_\rho (\partial_\rho + \rho^{-1}) v_\rho = 0$ . The solution to this equation is of the form  $v_\rho = a\rho + b\rho^{-1}$ . Using the boundary condition  $v_\rho(r_0) = 0$  at the outer septum boundary at  $\rho = r_0$ , we obtain  $v_\rho = -a\rho^{-1}(r_0^2 - \rho^2)$ . The septum stress is  $\sigma_{\rho\rho}(r) = \sigma_0 - 2\eta v_r r (1 + (r_0^2/r^2))/(r_0^2 - r^2)$ , which can

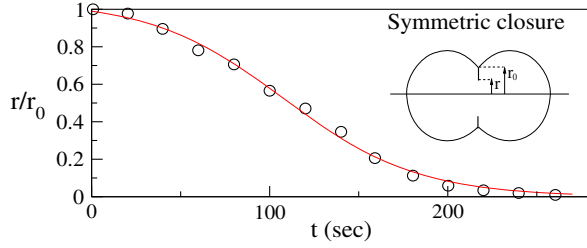


FIG. 3 (color online). Time evolution of the radius  $r$  of the contractile ring during cytokinesis. The circles are the experimental data of Ref. [5] obtained for *C. elegans* embryos, averaged over five embryos. The solid line is the best fit solution of Eq. (3) to the experimental data with  $r_0 = 14 \mu\text{m}$  and dimensionless parameters  $\tilde{\sigma} = 0.96$ ,  $\tau_0 \approx 38 \text{ s}$ , and  $\tilde{\zeta}_L^{-1} \approx 0$ .

be expressed in terms of the rate of change of the septum area  $A = \pi(r_0^2 - r^2)$ :

$$\sigma_{\rho\rho}(r) = \sigma_0 + \frac{\eta}{A} \frac{dA}{dt} \left( 1 + \frac{r_0^2}{r^2} \right). \quad (2)$$

The closure speed  $v_r = \dot{r}$  with  $v_r = -(a/r)(r_0^2 - r^2)$  is determined from the stress boundary condition normal to the inner edge of the septum at  $\rho = r$ . Because of radial symmetry the normal stress  $\sigma_{nn}(r) = -\sigma_{\rho\rho}(r)$  and  $\sigma_{nn}(r) + \Sigma/r = 0$ . This corresponds to a Laplace law in two dimensions. Note that in addition to a static part  $\Sigma_0$ , the line tension  $\Sigma$  may also contain a dissipative part corresponding to the effects of an intrinsic friction  $\zeta_L$ ,  $\Sigma = \Sigma_0 + (\zeta_L/L)(dL/dt)$ , where  $L = 2\pi r$  is the ring perimeter.

Combining Eq. (2) and the stress boundary condition, the dynamic equation for the radius  $r$  of the leading edge of the septum reads in dimensionless form

$$\frac{dx}{d\tau} = \frac{\tilde{\sigma}x - 1}{\frac{1}{x} + \frac{2}{\tilde{\zeta}_L} \frac{1+x^2}{1-x^2}}, \quad (3)$$

where  $x = r/r_0$ ,  $\tilde{\sigma} = (\sigma_0 r_0)/\Sigma_0$ ,  $\tilde{\zeta}_L = \zeta_L/(r_0\eta)$ , and  $\tau = t/\tau_0$  is the dimensionless time, with  $\tau_0 = \zeta_L/\Sigma_0$ . At late times when  $x \rightarrow 0$ , the rate of shrinkage  $dx/d\tau$  decreases exponentially as  $x(t) \approx \exp(-t/\tau_0)$ . An example of a solution to Eq. (3) is shown in Fig. 3 as a solid line.

Often, the septum closes asymmetrically [2,3], see Figs. 4 and 5(a). For simplicity we assume that the shape of an asymmetric septum is characterized by a circular arc  $c$  of radius  $R_s$  which intersects the initial furrow of radius  $r_0$ . The line tension of the contractile ring along the septum boundary  $c$  of length  $L$  is denoted  $\Sigma$ , and along the segment  $c'$  of length  $L'$  is denoted  $\Sigma'$ , see Fig. 4(c). Note that the line tensions  $\Sigma$  and  $\Sigma'$  both describe the contractile ring but differ because they correspond to different structures. The asymmetric septum is described by the potential  $E = 2\sigma A + \Sigma L + \Sigma' L'$ , where  $A$  is the septum area and  $\sigma$  is the surface tension of the septum membrane. The

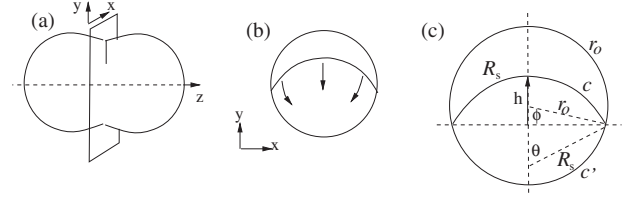


FIG. 4. Formation of an asymmetric septum during cleavage (a). Cross-sectional view of the furrow in the  $x$ - $y$  plane (b). Parametrization of the septum shape by angles  $\phi$ ,  $\theta$ , and height  $h$  (c).

position and shape of the inner edge of the septum, given by arc  $c$ , are fully determined by the angle  $\theta$  and the radius  $R_s$  or alternatively, by the angle  $\phi$  and the height  $h$  of the septum opening with boundary  $c$ , see Fig. 4(c). We obtain two coupled first order equations for  $h$  and  $\phi$  [12]:

$$\begin{bmatrix} L_h - \frac{fA_h}{\zeta_L} & L_\phi - \frac{fA_\phi}{\zeta_L} \\ \frac{BL_h}{L} & \frac{\tilde{\zeta}_\phi}{\zeta_L} + \frac{BL_\phi}{L} + 4\frac{\zeta_L'}{\zeta_L} \frac{1}{L'} \end{bmatrix} \begin{bmatrix} \dot{h} \\ \dot{\phi} \end{bmatrix} = \begin{bmatrix} (\tilde{\sigma}x - 1)L \\ -\left(2\frac{\Sigma_0'}{\Sigma_0} + B\right) \end{bmatrix}. \quad (4)$$

Here  $x = R_s/r_0$  is the dimensionless radius of the inner edge of the septum, and  $L_h = \partial L/\partial h$ ,  $L_\phi = \partial L/\partial \phi$ , and similarly for  $A_h$  and  $A_\phi$ . Furthermore,  $B = L_\phi + (1/x)A_\phi$ ,  $f = (xL\beta)/A$ , and  $\beta = 1 + (A_0/A_1)$ . Here  $A_0 = \pi r_0^2$  and  $A_1$  are the cross sectional area and the area enclosed by the ring, respectively. The motion of the corners [at the intersections of  $c$  and  $c'$ , see Fig. 4(c)] is described by the equation  $\zeta_\phi \dot{\phi} = -(\partial E/\partial \phi)|_A$ , where  $\zeta_\phi$  is a friction coefficient. In addition to the dimensionless parameters  $\tilde{\sigma} = \sigma_0 r_0/\Sigma_0$  and  $\tilde{\zeta}_L = \zeta_L/r_0\eta$  which govern the dynamics of the symmetric closure, we have introduced the parameter  $\tilde{\zeta}_\phi = \zeta_\phi/r_0^2\eta$ . Examples of numerical solutions to these equations as a function of time are shown in Figs. 5(b)–5(d).

We first compare our theory with experimental data on symmetric septum closure in *C. elegans* embryos (see Fig. 3) [5]. We fit solutions of Eq. (3) to the experimental data and estimate  $\tilde{\sigma} = \sigma_0 r_0/\Sigma_0 \approx 0.96$ ,  $\tau_0 = (\zeta_L/\Sigma_0) \approx 38 \text{ s}$ , and  $\tilde{\zeta}_L^{-1} \approx 0$ . The fact that  $\tilde{\sigma} \lesssim 1$  reveals that the contractile tension  $\Sigma_0$  is slightly above the value necessary to initiate septum closure against septum tension  $\sigma_0 r_0$ . Therefore, the closure speed is initially small. The estimate  $\tilde{\zeta}_L^{-1} \approx 0$  implies that internal line friction in the ring dominates over septum viscosity  $\zeta_L \gg \eta r_0$ . In this limit the solution to Eq. (3) is  $x(t) = [e^{t/\tau_0}(1 - \tilde{\sigma}) + \tilde{\sigma}]^{-1}$  which is shown as a solid line in Fig. 3. The characteristic time scale for symmetric septum closure is thus  $\tau_0 = \zeta_L/\Sigma_0$ .

We can estimate the parameter values of  $\sigma_0$ ,  $\Sigma_0$ , and  $\zeta_L$  as follows. Using  $\sigma_0 \approx 3 \times 10^{-4} \text{ N/m}$ , which was reported in experimental work on other eukaryotic cells [13], we estimate  $\Sigma_0 \approx 4.4 \times 10^{-9} \text{ N}$  and  $\zeta_L \approx 1.65 \times 10^{-7} \text{ N s}$ .

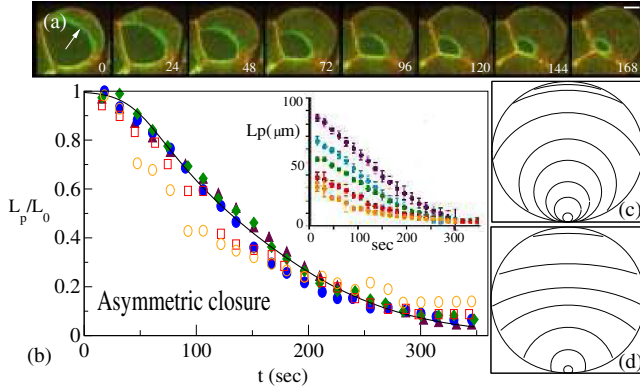


FIG. 5 (color online). Ring contraction during cytokinesis with an asymmetric septum. Fluorescence microscopy images of cytokinesis at different times (shown in seconds) in a *C. elegans* embryo in the four-cell stage [3] (a); scale bar  $5 \mu\text{m}$ . The contractile ring (see arrow) is stained by septin labeled green fluorescent protein. The septum emerges at the side of the cell which is not adhering to a neighboring cell. Quantification of the normalized perimeter  $L_p(t)$  of the ring as a function of time (b). The symbols distinguish different cell generations  $n$ . The inset shows original data from Ref. [3] for generations  $n = 1$  to 5 (top to bottom). The solid line is a fit of the solution to the equations for  $\dot{h}, \dot{\phi}$  to the data for  $n = 1, 2, 3$ , with  $r_0 = 14 \mu\text{m}$ ,  $\zeta'_L = \zeta_L$  and fit parameters  $\tilde{\sigma} = 1.43$ ,  $\tau_0 = 62.5 \text{ s}$ ,  $\Sigma'_0/\Sigma_0 = 2.5$ ,  $\tilde{\zeta}_L^{-1} \approx 0$ , and  $\tilde{\zeta}_\phi/\tilde{\zeta}_L \approx 0$ . Calculated septum shapes corresponding to the solid line in (b) [(c)]. Calculated septum shapes for smaller values of  $\tilde{\sigma} = 0.5$  and  $\Sigma'_0/\Sigma_0 = 1.5$  (d). Panel (a) and the inset of (b) are adapted from Ref. [3], with permission.

This estimate for  $\Sigma_0$  is consistent with estimates in other eukaryotes [14]. Further, using  $\eta \approx 10^{-3} \text{ Ns/m}$  [15], where the effective 2D viscosity  $\eta \approx \eta_{3D} \times w$ , with layer thickness  $w \sim 0.5 \mu\text{m}$ , we obtain  $\tilde{\zeta}_L^{-1} \approx 0.085$ , confirming that  $\tilde{\zeta}_L^{-1}$  is small compared to one as required by self-consistency.

We compare our theory to the experimentally observed asymmetric closure. Carvalho *et al.* have quantified the perimeter  $L_p = L + L'$  of the inner edge of the asymmetric septum as a function of time during cell division [see Fig. 5(a)] [3]. Data collected for successive cell divisions ( $n = 1, 2, \dots, 5$ ) starting from the fertilized egg ( $n = 1$ ) are shown in the inset of Fig. 5(b). The data show that the perimeter shrinks at a rate  $\dot{L}_p$  proportional to the initial perimeter  $L_0 \equiv L_p(t=0)$ . In Fig. 5(b) we represent  $L_p(t)/L_0$  as a function time, in which all the data collapse into a single curve. The normalized perimeter  $L_p/L_0$ , with  $L_0 = 2\pi r_0$ , is shown as a solid line. The best fit is obtained for  $\tilde{\zeta}_L^{-1} \approx 0$  and  $\tilde{\zeta}_\phi/\tilde{\zeta}_L \approx 0$ , which implies that in addition to  $\zeta_L \gg \eta r_0$ , as in the symmetric case, we also have  $\zeta_L \gg \zeta_\phi/\eta$ . This suggests that the friction  $\zeta_\phi$  is negligible compared to the intrinsic friction in the ring  $\zeta_L$ . Using  $\sigma_0 \approx 3 \times 10^{-4} \text{ N/m}$  as in the symmetric case, we estimate  $\Sigma_0 \approx 2.9 \times 10^{-9} \text{ N}$  and  $\zeta_L \approx 1.8 \times 10^{-7} \text{ Ns}$ . This corresponds to  $\tilde{\zeta}_L^{-1} \approx 0.076$ . The sequence of septum shapes

during closure that corresponds to the solid line in Fig. 5(b), is shown in Fig. 5(c). These shapes qualitatively resemble the experimentally observed shapes shown in Fig. 5(a). In Fig. 5(d) we show that using smaller values of  $\tilde{\sigma} = 0.5$  and  $\Sigma'_0/\Sigma_0 = 1.5$  in our calculations, the septum edge has a different shape with smaller curvature.

In this Letter we have developed a dynamical model to describe cytokinesis in animal cells, taking into account symmetric and asymmetric septum formation. By comparing our theoretical results with experimental data, we estimated parameter values that are relevant for the *C. elegans* embryo. The collapse of the time course of  $L_p(t)/L_0$  for different cell sizes implies scaling of the closure dynamics with respect to  $L_0$ ,  $\dot{L}_p(t) \sim L_0$ . In our theory scaling thus implies that  $L_p(t)/L_0$  is independent of  $r_0$ . For the case where  $\tilde{\zeta}_L \gg \tilde{\zeta}_\phi$  discussed here, this scaling is achieved if  $\Sigma_0$  and  $\zeta_L$  are both proportional to the initial septum radius  $r_0$ .

Scaling of  $\Sigma_0$  and  $\zeta_L$  with  $r_0$  is achieved if the properties of the contractile ring scale with cell size. This has also been suggested recently in a physical description of cytokinesis without septum formation [8]. Consistent with this idea it has been observed in other eukaryotes that the amount of myosin in the contractile ring increases with increasing cell size [16]. The scaling of both  $\Sigma_0$  and  $\zeta_L$  with  $r_0$  also implies that the time scale of closure  $\tau_0 = \zeta_L/\Sigma_0$  is independent of the cell size, as is indeed observed [see Fig. 5(b)].

Here, we have described the septum as a fluid sheet with effective tension  $\sigma_0 = 2\sigma'$  and viscosity  $\eta$ . Material properties [17] of the septum are difficult to estimate, also the source of the septum material is not clear. Material could arrive in the septum from the cytoplasm in small vesicles or it could flow from the plasma membrane, or both. Here we ignored the effects of confinement for septum formation. In the absence of confinement, septum formation requires that  $\sigma' < \sigma$ . This is the case if the septum is less contractile than the outer membrane or if the two membranes in the septum adhere [18,19]. Confinement allows for septum formation even in the absence of adhesion with  $\sigma' = \sigma$ . Interestingly, in the absence of the egg shell septum formation does not occur during the first division of the *C. elegans* embryo [20]. This suggests that in this division membrane confinement is relevant. At the same time, the estimated value of the furrow angle  $\psi \approx 120^\circ \pm 15^\circ$  (see Fig. A of Ref. [4]), implies the presence of significant adhesion at the mature septum. Note that confinement affects only the outer radius of the septum but not the dynamics of septum growth. We note that our theory could apply to other animal cells where division occurs via septation, but not to situations where a rigid cell wall is built to separate the daughter cells, as in fission yeast.

A. S. and M. M. I. acknowledge support from MPI-PKS, Dresden during their visits. A. S. also acknowledges useful discussions with G. Salbreux.

---

\*asain@phy.iitb.ac.in

- [1] Conventionally, the term septum is used for the new cell wall forming in bacteria or fission yeast during cell division. We use here the same term to refer to the new membrane interface forming in the absence of a cell wall in *C. elegans*.
- [2] H. Bringmann and A. A. Hyman, *Nature (London)* **436**, 731 (2005).
- [3] A. Carvalho, A. Desai, and K. Oegema, *Cell* **137**, 926 (2009).
- [4] A. S. Maddox, L. Lewellyn, A. Desai, and K. Oegema, *Dev. Cell* **12**, 827 (2007).
- [5] A. Zumdieck, K. Kruse, H. Bringmann, A. Hyman, and F. Jülicher, *PLoS One* **2**, e696 (2007).
- [6] M. Yoneda and K. Dan, *J. Exp. Biol.* **57**, 575 (1972).
- [7] D. Zinemanas and A. Nir, *J. Fluid Mech.* **193**, 217 (1988).
- [8] H. Turlier, B. Audoly, J. Prost, and J. F. Joanny, *Biophys. J.* **106**, 114 (2014).
- [9] M. P. Stewart, J. Helenius, Y. Toyoda, S. P. Ramanathan, D. J. Muller, and A. A. Hyman, *Nature (London)* **469**, 226 (2011).
- [10] F. Jülicher and R. Lipowsky, *Phys. Rev. E* **53**, 2670 (1996).
- [11] R. Albertson, B. Riggs, and W. Sullivan, *Trends Cell Biol.* **15**, 92 (2005).
- [12] Here we generalized the line tensions at arcs  $c$  and  $c'$  to be  $\Sigma = \Sigma_0 + (\zeta_L/L)(dL/dt)$  and  $\Sigma' = \Sigma'_0 + (\zeta'_L/L')(dL'/dt)$ , where  $\Sigma_0$  and  $\Sigma'_0$  are the contractile tensions along  $c$  and  $c'$ , and  $\zeta_L$  and  $\zeta'_L$  are corresponding dissipative coefficients. Motivated by Eq. (2) for the symmetric case, we use a simplified form of the stress in the case of asymmetric closure:  $\sigma_{nn} = \sigma_0 + (\eta/A)(dA/dt)(1 + (A_0/A_1))$ . The force balance equation at the inner edge is now  $\sigma_{nn} = \Sigma/R_s$ .
- [13] O. Thoumine, O. Cardoso, and J. J. Meister, *Eur. Biophys. J.* **28**, 222 (1999).
- [14] D. N. Robinson, G. Cavet, H. M. Warrick, and J. A. Spudich, *BMC Cell Biol.* **3**, 4 (2002).
- [15] G. Salbreux, J. Prost, and J. F. Joanny, *Phys. Rev. Lett.* **103**, 058102 (2009).
- [16] M. E. K. Calvert, G. D. Wright, F. Y. Leong, K.-H. Chiam, Y. Chen, G. Jedd, and M. K. Balasubramanian, *J. Cell Biol.* **195**, 799 (2011).
- [17] C. Guillot and T. Lecuit, *Dev. Cell* **24**, 227 (2013).
- [18] J.-L. Maitre, H. Berthoumieux, S. F. G. Krens, G. Salbreux, F. Jülicher, E. Paluch, and C.-P. Heisenberg, *Science* **338**, 253 (2012).
- [19] M. L. Manning, R. A. Foty, M. S. Steinberg, and E. M. Schoetz, *Proc. Natl. Acad. Sci. U.S.A.* **107**, 12517 (2010).
- [20] H. Koyama, T. Umeda, K. Nakamura, T. Higuchi, and A. Kimura, *PLoS One* **7**, e31607 (2012).